Cell Reports

Article

MYB68 regulates radial endodermal differentiation and suberin patterning

Graphical abstract

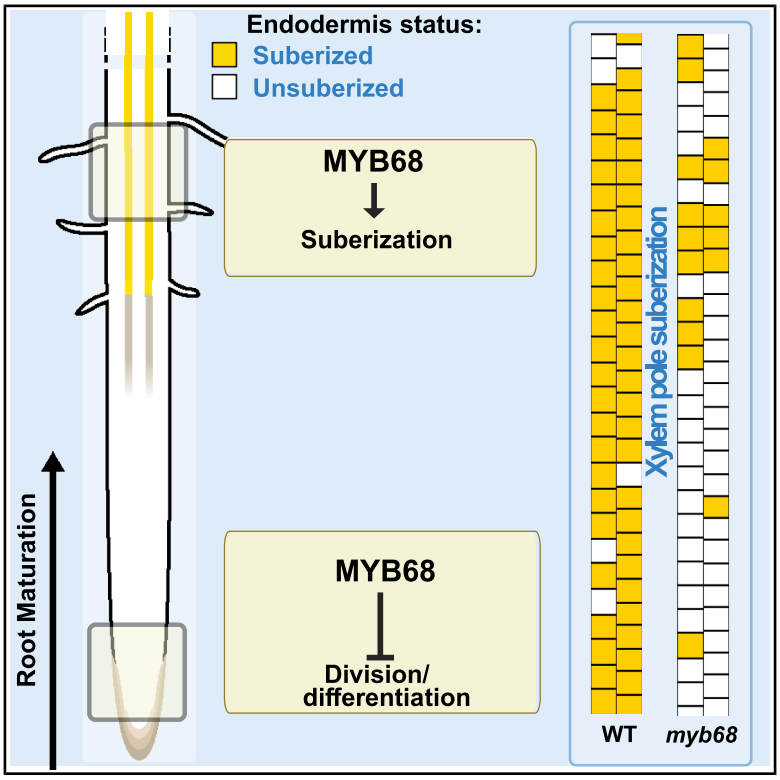

Authors

Leonie Kraska, Josep Mercadal Melia, Ryohei Thomas Nakano, David Molina, Pau Formosa-Jordan, Laura Ragni, Tonni Grube Andersen

Correspondence

tandersen@mpipz.mpg.de

In brief

In this study, Kraska et al. identify MYB68 as a novel regulator of endodermal suberization, linked to the formation of distinct identities in the xylem-pole-associated endodermis. The research uncovers new insights into the patterning of the endodermis with suberin and highlights genes encoding K-transport proteins associated with endodermal passage cells.

Highlights

- MYB68 regulates endodermal differentiation and controls suberin in distinct cell files
- The genetic program underlying endodermal suberization differs between cell files
- MYB68 represses the occurrence of endodermal passage cells
- A subset of K-transporters exhibits radially biased expression in the endodermis

Kraska et al., 2025, Cell Reports *44*, 115794
June 24, 2025
https://doi.org/10.1016/j.celrep.2025.115794

CellPress

Cell Reports

CellPress
OPEN ACCESS

Article

MYB68 regulates radial endodermal differentiation and suberin patterning

Leonie Kraska,[1] Josep Mercadal Melia,[1] Ryohei Thomas Nakano,[1,5] David Molina,[2,3] Pau Formosa-Jordan,[1,4] Laura Ragni,[2,3] and Tonni Grube Andersen[1,4,6,*]

[1]Max Planck Institute for Plant Breeding Research, Carl-von-Linne-Weg 10, 50829 Cologne, Germany
[2]ZMBP, Center for Plant Molecular Biology, University of Tübingen, Tübingen, Germany
[3]University of Freiburg, Institute of Biology II, Schänzlerstr 1, 79104 Freiburg, Germany
[4]Cluster of Excellence on Plant Sciences (CEPLAS), Cologne, Germany
[5]Present address: Department of Biological Sciences Faculty of Science, Hokkaido University, Hokkaido, Japan
[6]Lead contact
*Correspondence: tandersen@mpipz.mpg.de
https://doi.org/10.1016/j.celrep.2025.115794

SUMMARY

Roots are composed of concentric layers that surround the vasculature of plants. Of these, the endodermis stands out, as it contains barriers that facilitate selective uptake. In mature root regions, endodermal cells become coated with suberin, a hydrophobic polymer that seals off the inner root parts. Intriguingly, individual endodermal cells, adjacent to the water-conducting xylem, remain unsuberized. These cells are termed "passage cells," based on the assumption that they can facilitate vasculature access in an otherwise sealed-off area. The existence of passage cells suggests that distinct identities and cell files exist within the endodermis that may have overlooked importance. Here, we investigate this in the model plant *Arabidopsis thaliana*. Our work identifies a genetic regulator of cell-file-specific suberization and passage cell differentiation connected to the xylem. This provides spatiotemporal insights into the mechanism(s) underlying suberization, establishing a framework for the radial organization of the endodermis and highlighting the putative function(s) of passage cells.

INTRODUCTION

The organization of root cell layers is crucial for selective filtering of solutes translocated between the above- and below-ground plant parts. In the model plant *Arabidopsis thaliana* (hereafter *Arabidopsis*), the outer tissues comprise the soil-facing epidermis (or rhizodermis) and two underlying cell layers: the cortex and the endodermis, which together constitute the ground tissue.[1] The endodermis has historically received the most attention, as it contains apoplastic diffusion barriers that are key for the selective uptake of minerals and nutrients.[2] In contrast to the radially symmetric outer layers, the central vasculature is organized in opposing xylem and phloem poles, facilitating upward water/mineral and downward sugar transport, respectively. Anatomically, the endodermis overlays the vasculature, and the individual files within its circumference largely align with these vascular poles. Thus, the radial organization of endodermal cells can be divided into those that are xylem pole-associated (XPE), phloem pole-associated (PPE), or situated between the two poles (non-pole-associated [NPE]). No distinct function has yet been ascribed to these files, but after about 1 week of growth, sporadic formative divisions in the early XPE cells initiate an additional ground tissue layer called the middle cortex (MC).[3] The existence of MC suggests that XPE cells contain specialized developmental information related to their xylem-associated position.[3,4] A second cortex cell layer has also been described in the hypocotyl and the root-shoot junction of young roots,[5] but it remains unknown if this is also initiated in the XPE.

As the root grows and cells exit the meristematic root tip, the endodermis undergoes two stages of differentiation before dying off during periderm formation.[2,6] The first involves the deposition of a lignin-based apoplastic barrier known as the Casparian strip (CS).[7] The CS prevents extracellular diffusion and forces the movement of solutes across the endodermal plasma membrane.[8] The second stage is characterized by the deposition of the hydrophobic polymer suberin in the form of a lamella-like structure across the entire cell surface.[9,10] Suberin blocks transport across the plasma membrane and thereby seals off the vasculature.[11]

In 5- to 6-day-old *Arabidopsis* seedlings, suberization occurs approximately 15–20 cells after the formation of the CS and follows a stereotypical pattern along the longitudinal root axis.[12] In this area of the root, the decision to suberize appears sporadic and is typically initiated slightly earlier in PPE than in XPE and NPE cells.[13] This gives rise to a so-called "patchy zone" of about 10–15 endodermal cells along the longitudinal axis, where not all cells across the endodermal circumference are suberized. Shootward to this point, a "fully suberized" zone is established, covering the remaining endodermis to the root-hypocotyl

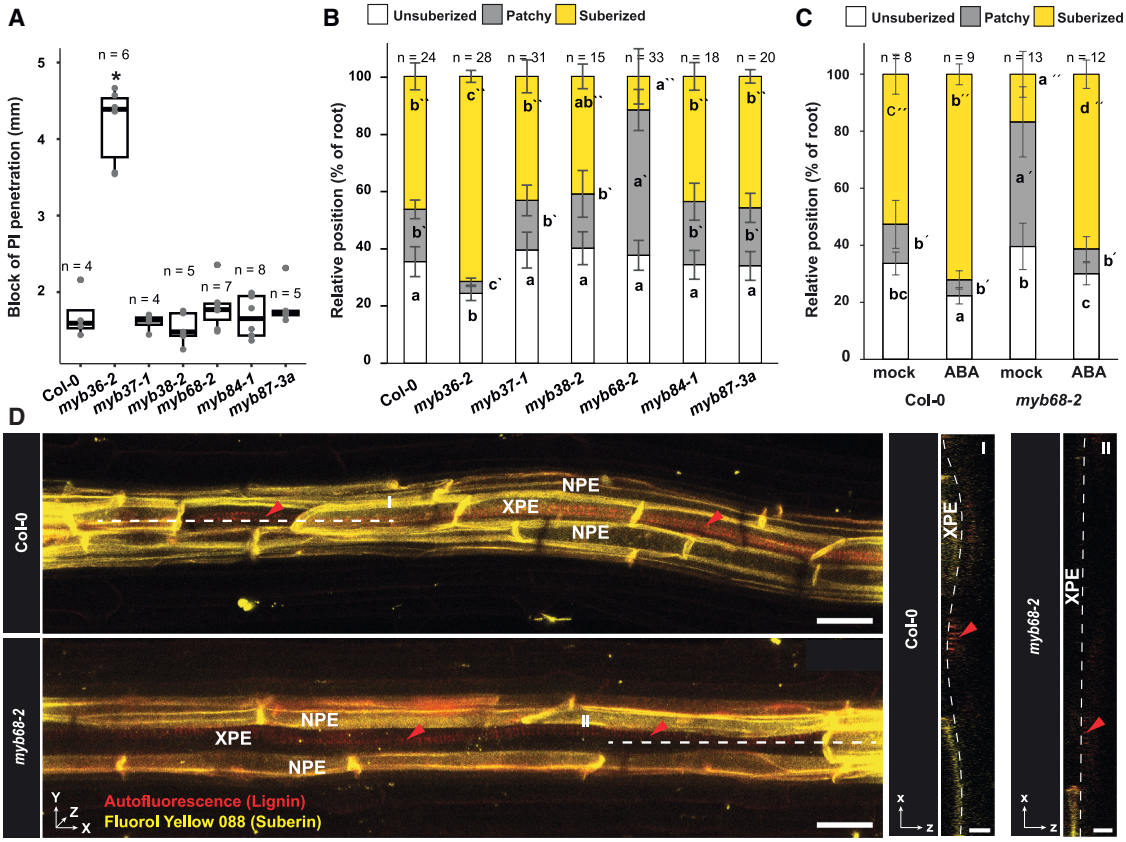

Figure 1. Formation of endodermal barriers in MYB36-clade mutants

(A) Functional analysis of CS by measuring the onset of PI diffusion blockage into the stele.[21] Asterisks depict significant differences compared to the wild type (WT) according to an unpaired Wilcoxon test.

(B and C) Suberization patterning in 6-day-old roots stained with fluorol yellow 088 (FY).

(D) Confocal projections of the suberized zone (approximately 60% relative position) of Col-0 and *myb68-2* root stained with FY. Lignin was imaged by measuring autofluorescence after excitation using a 405 nm laser. Individual letters depict significance ($p < 0.05$) according to a Kruskal-Wallis test with a post hoc Nemenyi test. Letters without a prime refer to unsuberized zones, letters with one prime refer to patchy zones, and letters with two primes refer to fully suberized zones. For the boxplot in (A), the center line indicates the median, dots represent data points, the box limits represent the upper and lower quartiles, and the whiskers represent the maximum and minimum values. For barplots, data are represented as the mean, and error bars depict the standard deviation. The scale bar represents 100 μm. ABA, abscisic acid; NPE, non-pole-associated endodermis; PI, propidium iodide; XPE, xylem pole-associated endodermis.

junction. Intriguingly, and in line with distinct radial functions within the endodermis, a few individual cells in the XPE and NPE remain unsuberized.[13–15] These are referred to as endodermal "passage cells" (PCs) because their lack of suberization is thought to provide a low-resistance radial flow path for nutrients and water into the xylem.[15] Although PCs were identified over a century ago and have been observed in many plant lineages,[14] genetic insights into their function and development have only recently begun to emerge. In *Arabidopsis*, the first steps toward PC formation are initiated in the meristematic XPE by radially organized hormone-related signals emanating from the developing xylem.[13,16] However, the spatially distinct genetic network downstream of this decision, as well as mechanisms that initiate the decision to suberize within the individual endodermal cell, remains unknown.

In this study, we set out to find factors that control radial endodermal differentiation toward suberization with a focus on gaining insights into PC specification. Our work identifies the myeloblastosis (MYB)-class transcription factor (TF) MYB68, a homolog of the CS master regulator MYB36, as an important player for distinct suberization patterns in the XPE and NPE endodermal cell files. Through transcriptional profiling, we highlight that MYB68 is involved in a genetic network that regulates XP-associated ground tissue differentiation. We find that MYB68 likely functions in both mature and young endodermal cells, where it is implicated in an age-dependent mechanism that determines the suberization status as well as the formation of MC and PCs. Combined, these results bring about insights into root cell identity establishment and provide tools for a deeper understanding of spatiotemporal patterning and functions.

RESULTS

MYB68 influences endodermal suberization

To start our investigation, we focused on a subclade of MYB TFs that includes the master regulator of CS formation, MYB36.[17,18]

We hypothesized that within this clade, other members may play roles associated with endodermal differentiation. This subfamily comprises six members: MYB36, MYB37, MYB38, MYB68, MYB84, and MYB87, for which we recently established homozygous knockout (KO) mutant lines.[19] For MYB68, a previous study identified a KO allele in the Landsberg ecotype,[20] and we therefore named our alleles *myb68-2* and *myb68-3*. To assess whether mutants of this clade of MYBs are affected in endodermal development, we examined the functionality of the CS and measured suberin patterning in 6-day-old roots. Consistent with previous findings,[17,18] *myb36-2* exhibited a dysfunctional apoplastic barrier, evidenced by a significant increase in propidium iodide (PI) penetration into the vasculature[21] (Figure 1A). *myb36-2* also displayed an early suberization onset, which is associated with its impaired CS function[22] (Figure 1B). Besides these well-established defects, only *myb68* alleles exhibited changes in relation to endodermal barrier formation (Figures 1B, S1A, and S1B). This manifested as a significant increase in the relative size of the patchy suberized zone (Figure 1C), which occurred mainly within the XPE (Figure 1D). This cell-file-specific absence of suberin could be significantly reduced by complementing the *myb68-2* mutant with the genomic region of the MYB68 allele (Figures S1C and S1D).

To investigate whether this role of MYB68 was related to a general defect in the ability to synthesize or deposit suberin, we exposed *myb68* roots to 1 μM abscisic acid (ABA) for 2 days to induce endodermal suberin deposition.[23] This resulted in a significantly earlier onset of coherent suberin deposition in the roots of Col-0 and both of our *myb68* alleles across all cell files (Figures 1C and S1B). Taking these results together, we therefore conclude that MYB68 most likely functions in a genetic network that influences the decision of endodermal cells to undergo suberization rather than directly controlling the biosynthesis or deposition machinery.

Suberin deposition displays cell-file-specific MYB68-dependent dynamics

To further investigate the cell-file-associated decrease of suberin in *myb68* plants, we measured the entire circumferential suberin status of the individual cells within the distinct files (XPE, NPE, and PPE) in 6-day-old roots (Figure 2A). As we observed a similar overall suberin pattern in both *myb68-2* and *myb68-3* (Figure S1B), we focused this detailed analysis on *myb68-2*. By plotting the cumulative sum of suberized cells against their relative position along the longitudinal axis, we could assess the suberization continuity from onset until the root-hypocotyl junction (for a detailed description, see the STAR Methods). In both Col-0 and *myb68-2* roots, PPE cell files gave rise to a linear behavior, although deviations could be observed in *myb68-2* due to the presence of a few unsuberized cells (Figure 2A). For NPE cell files, both genotypes displayed a bilinear trend, reflecting the patchy and fully suberized zones, respectively. In XPE and, to a lesser extent, NPE files, the suberization frequency was reduced in *myb68-2* roots when compared to Col-0 (Figure 2A). MYB68 therefore appears to primarily influence suberization in XPE and NPE cell files, thereby playing a role in the regulation of the patchy zone. One intriguing additional observation was that Col-0 roots consistently had a decrease in the number of suberized cells in XPE and NPE files at the upper end of the roots close to the hypocotyl (Figure 2A), suggesting that an unsuberized area exists at this developmental stage.

We next measured the progression of suberization from 3- to 11-day-old roots, which cover the entire endodermal lifespan.[6,24] In both Col-0 and *myb68-2*, the fully suberized area correlated positively with root length (Figures 2B and 2C). Since both the aging endodermal cells and the periderm are suberized, this zone must make up an increasing proportion as the root grows.[6] The length of unsuberized and patchy areas also increased with age (Figures 2B and 2C), with the latter stabilizing when roots reached a length of approximately 20 mm (Figure 2C). As these zones are assumed to be coordinated with the formation of new cells and thus root growth, this dynamic behavior suggests that age-dependent mechanism(s) may additionally influence the decision to suberize. Since *myb68-2* roots displayed a delay in full suberization but had a similar patterning rate and onset to Col-0 (Figures 2B and 2C; Table S1), MYB68 likely plays a role in such an age-dependent network.

MYB68 controls occurrence of endodermal PCs

Since primarily XPE cells showed delayed suberization in *myb68-2* (Figures 1D and 2A), changes in PC occurrence may also explain the increased patchy zone of *myb68-2*. These cells are typically defined by their lack of suberin and therefore indistinguishable from unsuberized cells, rendering them difficult to assess. Several genes have been described as being expressed in PCs, including *PHOSPHATE EXPORTER HOMOLOG 3* (*PHO1;H3*).[13,14] We therefore used a transcriptional marker for this gene (p*PHO1;H3*:NLS 3xmVenus) and measured its activity in the zone of the endodermis, which normally undergoes suberization. Mainly cells in the XPE and NPE of wild-type roots displayed *PHO1;H3* activity, which was significantly increased in *myb68-2* roots (Figures 3A and 3B). Thus, MYB68 may repress PC identity. In support of this, germination of *myb68-2* on PC-suppressive concentrations of the artificial cytokinin 6-benzylaminopurine (BAP)[13] led to a dose-dependent reduction in PC occurrence within the suberized zone of Col-0, which was exaggerated in *myb68-2* roots (Figures 3C and 3D).

A subset of transporter-encoding genes is associated with PCs

Based on the apparent increase in PC occurrence in *myb68* roots, we next set out to probe if this finding could give insights into their transcriptional identity. We reasoned that, in our growth setup, genes with expression associated with PCs would have to fulfill two criteria: (1) exhibit increased expression in *myb68-2* when compared to Col-0 and (2) display Col-0-like expression levels upon BAP treatment, as this restored *myb68-2* suberization back to a similar pattern to that observed in mock-treated Col-0 (Figure 3C). 296 genes were significantly upregulated in *myb68-2*, of which 66 showed repression upon BAP treatment (Figure 4A; Tables S2 and S3). This subset did not include *PHO1;H3*, possibly due to PC-associated expression being masked by its strong expression in the stele.[13,26] Thus, our selection criteria probably define more specific PC-associated components and overlook genes with wider expression patterns. Despite this limitation, a Gene Ontology (GO) term analysis of

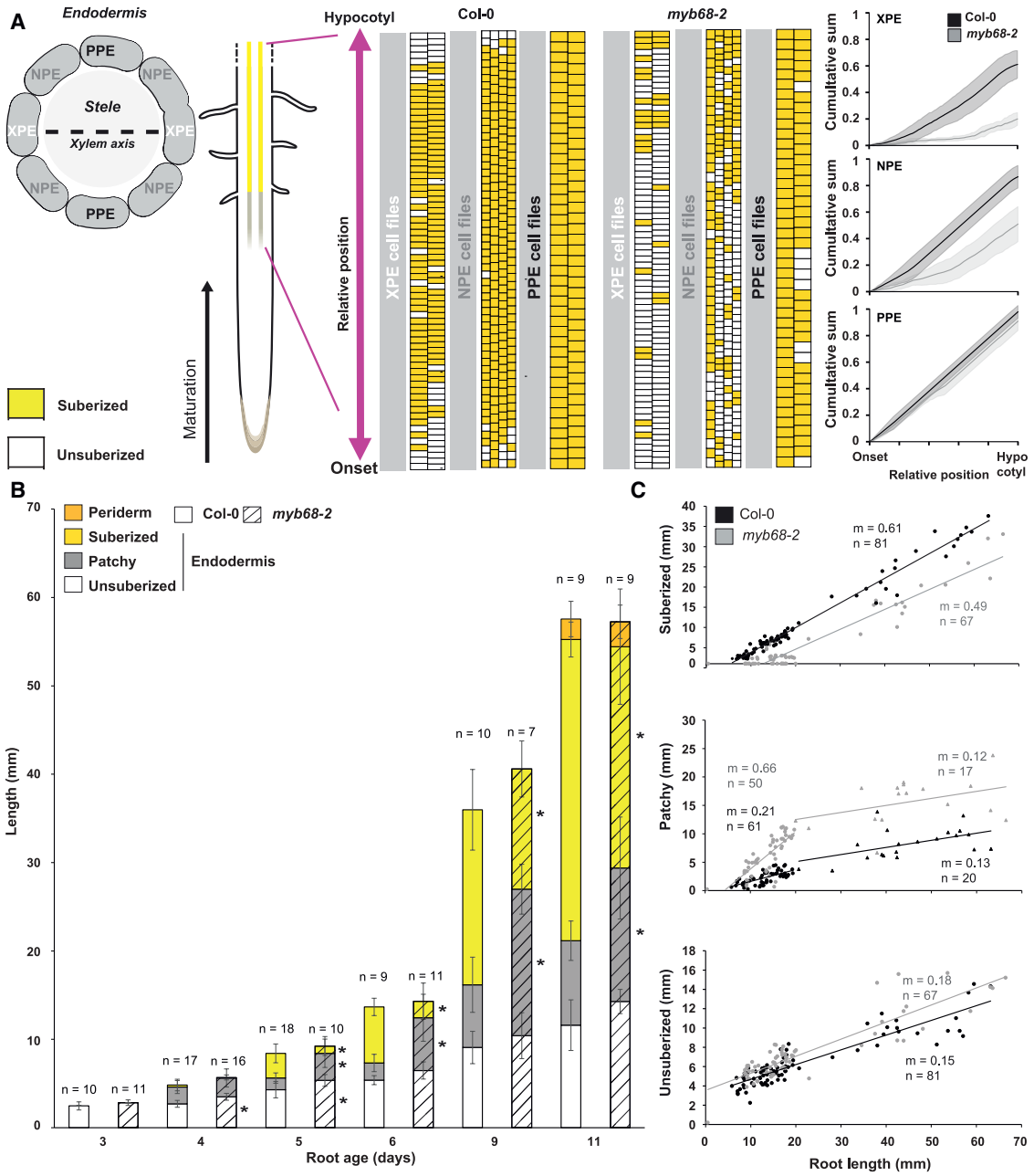

Figure 2. Spatiotemporal analysis of endodermal suberization patterns

(A) Analysis of radial suberin patterning of roots stained with fluorol yellow 088 (FY). The cumulative sum of each cell file along the upper 50% of the root was plotted for WT and *myb68-2* against the position on the longitudinal axis (STAR Methods). Every square represents a cell. The lines in the graphs depict the average of cell files across 3 individual roots, and shading represents the standard deviation (SD).

(B) Time-course analysis of suberin patterning in roots from 3 to 11 days of age stained with FY. Asterisks indicate significant differences between Col-0 and *myb68-2* at each time point and in each zone via an unpaired Wilcoxon text (*$p < 0.05$).

(C) Data from (B) plotted to reveal the relationship between suberin zones and root length from 3- to 11-day-old roots.

For barplots, data are represented as the mean, and error bars depict the SD. Lines depict a linear regression fit with calculated values for the slopes (m) (see Table S1). In (A), the shading depicts SD. XPE, xylem pole-associated endodermis; PPE, phloem pole-associated endodermis; NPE, non-pole-associated endodermis.

the 66 PC-associated candidates[27] showed significant enrichment in functions such as "inorganic cation transmembrane transport," "response to gibberellin," and "regulation of cell communication and signaling" (Figure 4B). This is in line with the previously proposed roles of PCs in nutrient homeostasis and biotic communication.[14,15]

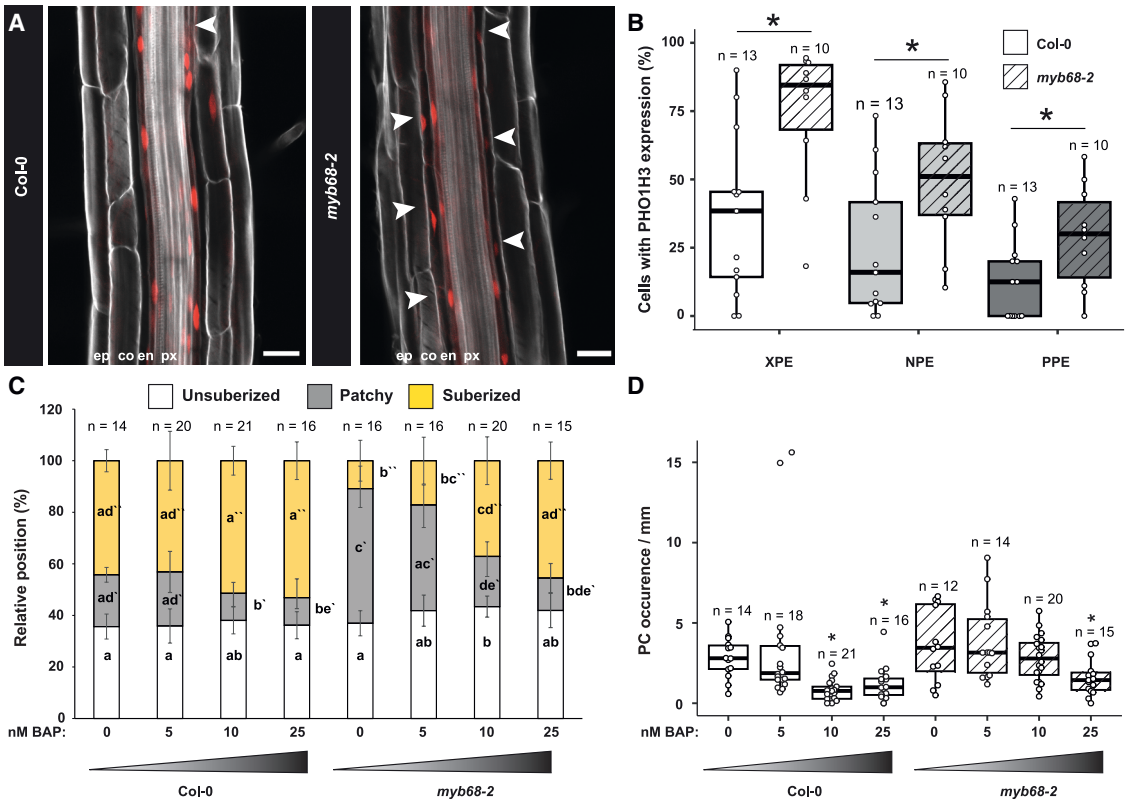

Figure 3. Investigation of passage cell occurrence in the *myb68-2* mutant

(A) Representative root of a transcriptional marker line reporting activity of the promoter region of a *PHO1;H3* (*pPHO1;H3:NLS 3xmVenus*).[13] Image originates from the upper 50% of a 6-day-old root. Arrowheads highlight endodermal cells with signal. *PHO1;H3* activity is depicted in red, and the cell walls were stained with calcofluor white (gray) according to Ursache et al.[25]

(B) Proportion of endodermal cells with expression of *PHO1;H3* in the XPE, NPE, or PPE in the upper 50% of the root. Each data point represents the percentage within each analyzed root. Asterisks indicate significant difference between *PHO1;H3* activity in the WT (pGPAT5:mCitrine-SYP122)[13] and *myb68-2* background lines in each longitudinal position according to an unpaired Wilcoxon test (*$p < 0.05$).

(C) Suberization pattern in roots grown in the presence of increasing amounts of the artificial cytokinin 6-benzyl-aminopurine (BAP). For boxplots, the center line indicates the median, dots represent data points, the box limits represent the upper and lower quartiles, and the whiskers represent the maximum and minimum values. For barplots, data are represented as the mean, and error bars depict the standard deviation. Individual letters depict significance ($p < 0.05$) according to a Kruskal-Wallis test with a post hoc Nemenyi test. Primes refer to zones of suberization status.

(D) Passage cell (PC) occurrence in roots from (C). Asterisks indicate significant differences between mock- and BAP-treated samples in an unpaired Wilcoxon text (*$p < 0.05$). XPE, xylem pole-associated endodermis; PPE, phloem pole-associated endodermis; NPE, non-pole-associated endodermis.

Within the transport-related GO term, we focused on the two potassium (K) transporters *POTASSIUM UPTAKE 8* (*KUP8*) and *HIGH AFFINITY K+ TRANSPORTER 5* (*HAK5*),[28,29] as well as the *Arabidopsis* sodium (Na) transporter *HIGH-AFFINITY K+ TRANSPORTER 1* (*HKT1*)[30] (Figure 4C; Table S4). To determine whether the expression of these genes is indeed associated with PCs, we created promoter-based transcriptional marker lines or performed whole-mount hybridization chain reaction fluorescent *in situ* hybridization (HCR-FISH).[31] Interestingly, in the suberizing part of 6-day-old Col-0 roots, p*KUP8* showed activity in the endodermis, pericycle, and specifically the inner cortex cells close to the hypocotyl where two layers had formed (Figures 4D and S2A). *HAK5* mRNA was localized in the endodermis and most cortex cells (including those close to the hypocotyl) (Figures 4D and S2C), whereas *HKT1* displayed activity across all the investigated tissues (Figures 4D, S2B, and S2D). Upon quantification, the expression of *KUP8* showed a bias toward XPE and NPE cells and was significantly increased in the *myb68-2* mutant across all endodermal cell files (Figure 4D). For *HAK5*, although its expression was equally present across cell files in Col-0, specifically XPE, NPE, and cortex cell files displayed a significant increase of expression in *myb68-2*. For *HKT1*, only endodermal expression was significantly increased in *myb68-2* (Figures 4D, S2D, and S2E). Combined, these analyses provide novel candidate genes that are likely associated with PC function and highlight a potential role of these elusive cells in cation homeostasis.

MYB68 represses endodermal division in the apical meristem

Within the subset of genes with PC-correlated expressional behavior, we additionally observed several related to gibberellin signaling, as well as the MC-associated *SCARECROW-LIKE 3* (*SCL3*)[32,33] (Figure 4C). Thus, MYB68 may additionally influence

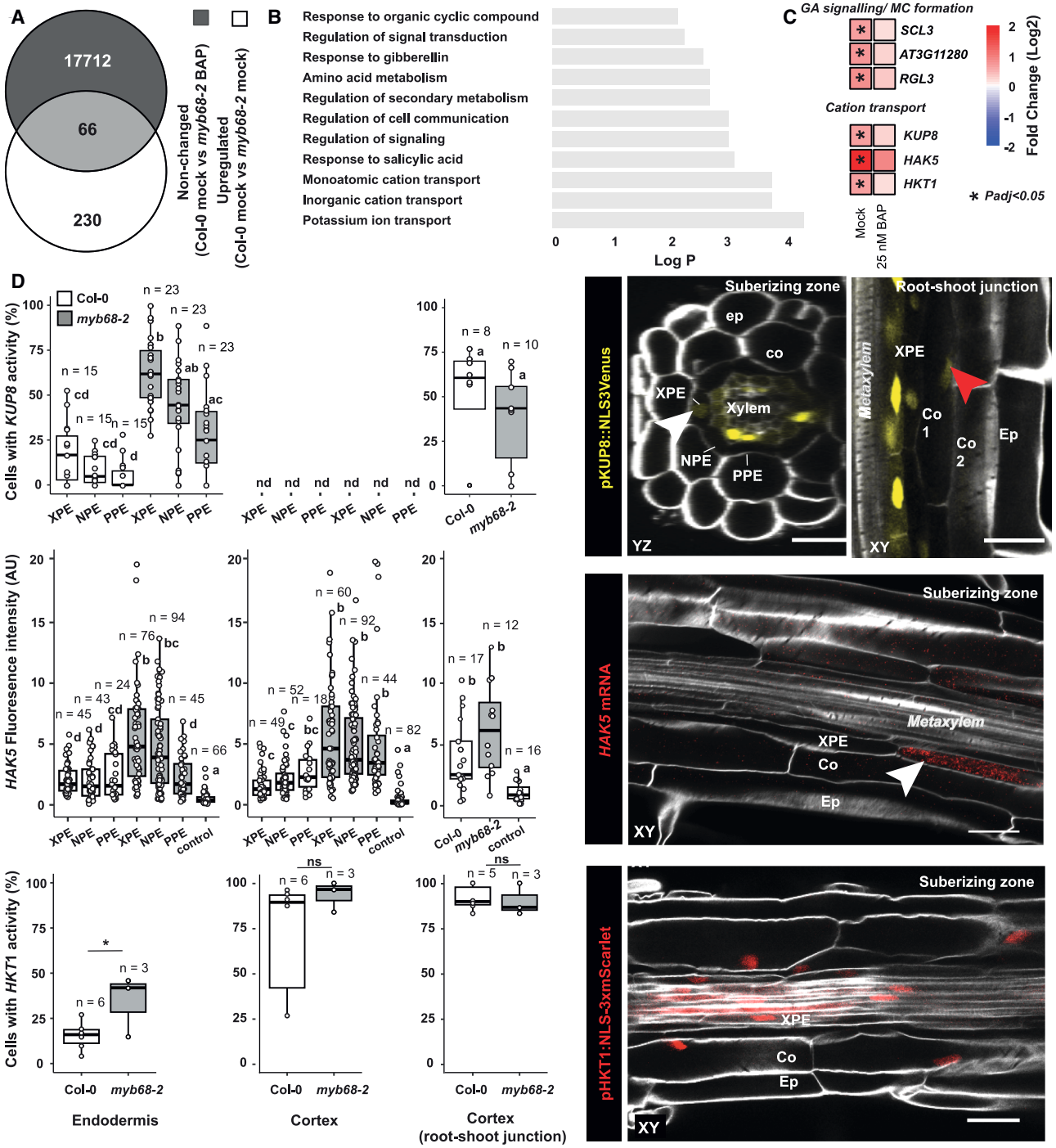

Figure 4. Passage cell-associated transcriptional analysis

(A) Overlap of upregulated genes in 6-day-old Col-0 vs. *myb68-2* roots (p_{adj} < 0.05) and genes with non-significant changes in Col-0 vs. *myb68-2* when germinated on 6-benzyl-aminopurine (BAP; 25 nM).

(B) GO term analysis of the 66 overlapping genes from (A).

(C) Heatmap of selected gibberellic acid (GA)- and middle cortex (MC)-associated genes as well as cation transporters in the comparisons from (A) (all genes are shown in Tables S4 and S5).

(D) Transcriptional activity of gene expression in the endodermis and cortex at approximately 75% relative position of the root as well as in the inner cortex close to the root-shoot junction. Expression analysis of *KUP8* and *HKT1* in Col-0 and *myb68-2* was performed using fluorescent transcriptional marker lines (expressing *pKUP8*:NLS3xVenus or *pHKT1*:NLS-3xmScarlet, respectively). Each data point represents the percentage of cells with expression in individual roots (a minimum

(legend continued on next page)

hormonal responses associated with the formation of MC in the meristematic XPE file. To analyze this, we grew plants for 6 days on agar plates with a mesh filter, as this provided a more consistent establishment of MC under our growth conditions. In line with our transcriptomic analysis, *myb68-2* and *myb68-3* mutants displayed a significant increase in MC occurrence (Figures 5A, 5B, and S1E), suggesting that MYB68 may also be involved in repressing the formation of these cells in XPE files.

MYB68 is expressed in both differentiated and meristematic tissues

The influence of MYB68 on MC formation is intriguing, as this suggests an additional role for MYB68 in coordinating suberization patterning and periclinal division of the XPE cells in the undifferentiated apical root meristem. We therefore aimed to characterize the expression pattern of MYB68. For this, we constructed fluorescent reporter lines to investigate both transcriptional and translational expression. Our constructs utilized the full intergenic region (p*MYB68*) upstream of *MYB68* to drive the expression of a nuclear-localized fusion reporter (*pMYB68*:NLS 3xmVenus) or a *myb68*-complementing genomic DNA fragment encoding MYB68 fused N-terminally to GFP (Figures S1C and S1D). Consistent with a local effect on suberization, both reporters displayed activity in the endodermis and in other vascular-associated cells in the root regions corresponding to the suberized zone (Figures 6A and 6F). Our translational reporter also showed the accumulation of GFP-MYB68 in the endodermis, pericycle, and vascular tissues in the elongation zone (Figure 6F). However, only the p*MYB68* reporter showed additional activity in the proximal meristem (Figures 6A and 6F). Here, PPE cells exhibited activity immediately after the formation of the cortex-endodermis initial daughter cells (CEIDs), whereas the onset of activity in XPE and NPE cells was significantly delayed (Figures 6A, 6B, S3A, and S3B). This radial difference in transcriptional activity was dose-dependently repressed by BAP concentrations that affect PC occurrence (Figures 6C and S3C). Furthermore, the onset of p*MYB68* activity shifted toward the distal meristematic cells as the root aged (Figures 6D, 6E, S3D, and S3E). Taken together, these observations suggest that, in addition to its probable role in regulating suberization at the single-cell level, MYB68—or its transcript—may also influence mechanisms related to XPE differentiation in the meristematic region.

DISCUSSION

In this work, we provide evidence that the MYB-class TF MYB68 functions within a genetic network regulating the radial establishment of endodermal suberization. This expands on a recent finding that suggested MYB68 directly activates suberin-related gene expression in the periderm.[19] Indeed, we observed MYB68 expression in pericycle cells, most likely reflecting its role in periderm formation (Figure 6). However, a deeper analysis revealed that in roots not yet undergoing secondary growth, MYB68 is active not only in endodermal cells destined for suberization but also in the nuclei of cells outside the suberizing region, specifically in the elongation zone (Figure 6). Thus, before the onset of secondary growth, MYB68 most likely plays a role in initiating and maintaining the suberization process. Given that MYB factors can form protein complexes,[34] it is plausible that MYB68 interacts with distinct partners to generate context-dependent functional outputs. Such an organization would enable MYB68 to regulate differentiation and suberization through distinct regulatory assemblies in different root domains.

Intriguingly, our analyses also link MYB68 to a previously established model for PC formation in the proximal meristem. In this model, hormone-based mechanisms that enable and maintain xylem and phloem identities in the vasculature[35] extend to the endodermis. This vascular-associated imprint on endodermal cells directs PPE cells toward a differential fate that culminates in early suberization, while xylem-specific hormonal patterns guide XPE (and NPE) cells to follow a different trajectory (i.e., PC formation).[13] Thus, the positive role of MYB68 on the suberization process, along with its earlier onset of expression in PPE cells, may reinforce the pathway leading to suberization in these cell files. Conversely, delayed expression in the XPE could permit distinct differentiation associated with PC formation. Since we were unable to detect MYB68 accumulation in the meristematic region, this regulatory role may not occur at the protein level. Alternatively, MYB68 may be rapidly degraded in these cells. In support of the latter, MYB factors related to hormonal signaling have been described as targeted for swift turnover.[36]

One additional observation was that *myb68* roots exhibit an earlier onset of MC formation in the meristem than Col-0 (Figure 5). Thus, similar to what has been proposed for the periderm,[19] MYB68 might suppress periclinal divisions in the young ground tissues. This is consistent with the PPE-biased p*MYB68* activity in the meristem, as its expression in this region could underlie the inhibition of MC formation in these cells.[3] Interestingly, we also found evidence that the onset of promoter activity in the meristem is age dependent, eventually disappearing from the meristematic endodermis (Figure 6D). This proposes that MYB68 likely serves to connect age-dependent periclinal divisions, such as MC formation,[3] with suberin patterning in the endodermis (Figure 2B). Indeed, a recent study demonstrated that the *Arabidopsis* meristem undergoes juvenile and adult phases.[37] Thus, phases may include a MYB68-containing regulatory network that integrates meristem age, XPE divisions, and suberization patterns in the mature root based on the progression of meristematic age (Figure 7).

The observation that the presumptive PC occurrence is increased in *myb68* roots further allowed us to investigate their

7 cells per root). For *HAK5* mRNA, fluorescence *in situ* hybridization was employed. As negative control, either a probe specific for a bacterial gene (dapB, *Bacillus subtilis*) with the corresponding amplifier or only the amplifier used for HAK5 without a probe was used (see STAR Methods). For boxplots, the center line indicates the median, dots represent data points, the box limits represent the upper and lower quartiles, and the whiskers represent the maximum and minimum values. Individual letters show significance according to a Kruskal-Wallis test with a post hoc Nemenyi test. XPE, xylem pole-associated endodermal cells; PPE, phloem pole-associated endodermal cells; NPE, non-pole-associated endodermal cells; Ep, epidermis; Co, cortex; En, endodermis; nd, not detected; ns, not significant. Scale bars represent 25 μm.

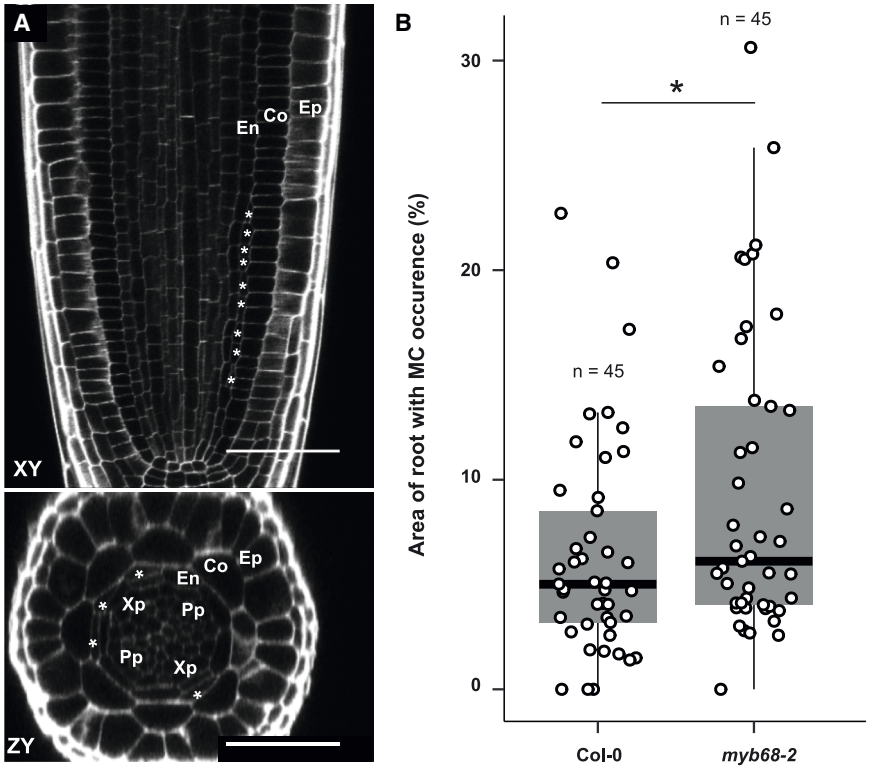

Figure 5. Middle cortex cell occurrence in 6-day-old *myb68-2* roots

(A) Representative image of a longitudinal (*xy*) and transversal (*zy*) section of a 6-day-old *myb68-2* meristem with middle cortex (MC) occurring. Cell walls were stained with calcofluor white (gray) according to Ursache et al.[25] Asterisks indicate MC cells.

(B) Measurement of MC occurrence in 6-day-old roots. The graph depicts the percentage of root with MC occurrence. Ep, epidermis; Co, cortex; En, endodermis; Pp, phloem pole; Xp, xylem pole. In (B), the center line indicates the median, dots represent data points, the box limits represent the upper and lower quartiles, and the whiskers represent the maximum and minimum values. Asterisks indicate significant difference compared to Col-0 according to an unpaired Wilcoxon text (*$p < 0.05$). Scale bars represent 50 μm.

function. Our finding that several transporter-coding genes are associated with the changed PC behavior in *myb68-2* supports their proposed role(s) in nutrient and ion homeostasis.[14,26,38,39] Notably, our identified candidates included transporters related to K+/Na+ homeostasis, suggesting that PCs (or non-PPE cells) may play a role in cation regulation. Since MC formation is enhanced upon abiotic stress conditions,[40] MYB68 may coordinate developmental mechanisms that help alleviate stress conditions in the root. *HKT1*, *KUP8*, and *HAK5* were all expressed at the junction between the root and the hypocotyl, a region that shows less frequent suberin deposition in Col-0 roots and forms a second cortex layer[5] (Figures 4D and S2C–S2E). We speculate that this zone may function to sequester toxic ions in the ground tissue, which is shed during secondary growth and periderm formation. By transporting toxic compounds from the vasculature into cortex cells via PCs, this mechanism could enable the root to expel unwanted ions by directing them into cells that will be removed upon periderm formation. While this hypothesis requires deeper physiological investigation, it suggests a potentially overlooked role for PCs in root function, particularly in cation homeostasis and abiotic stress tolerance.

Limitations of the study

One limitation of this study is that the precise targets of MYB68 remain unknown, preventing us from inferring its direct functions. The presence of MYB68 in multiple tissues suggests diverse roles in root development, which will require much deeper analysis to fully understand. While our findings highlight the dynamic nature of endodermal suberization patterns, the underlying genetic networks driving these processes cannot be fully elucidated from our current data. Additionally, although we have explored potential roles of PCs in cation homeostasis, we provide no physiological evidence to directly support this hypothesis.

RESOURCE AVAILABILITY

Lead contact

Further information and requests for resources and reagents should be directed to and will be fulfilled by the lead contact, Tonni Grube Andersen (tandersen@mpipz.mpg.de).

Materials availability

Materials newly produced in this work are available from the lead contact upon reasonable request.

Data and code availability

- RNA sequencing (RNA-seq) raw reads generated in this study have been deposited at the National Center for Biotechnology Information under BioProjectID: PRJNA1110212. Sequence data for *Arabidopsis* genes used in this study can be found in The Arabidopsis Information Resource (www.arabidopsis.org) under the following accession numbers: At4g13420 (*HAK5*), At4g10310 (*HKT1*), At5g57620 (*MYB36*), At5g57620 (*MYB37*), At2g36890 (*MYB38*), At5g65790 (*MYB68*), At4g37780 (*MYB84*), At3g49690 (*MYB87*), At5g14880 (*KUP8*), At1g 14040 (*PHO1;H3*), At5g17490 (*RGL3*), and At1g50420 (*SCL3*).
- This paper does not report any original code.
- Any additional information required to reanalyze the data reported in this paper is available from the lead contact upon request.

ACKNOWLEDGMENTS

All authors thank Ton Timmers and the Central Microscopy facility (CeMic) for microscopy aid. Aristeidis Stamatakis and his greenhouse team at MPIPZ are thanked for help with plant growth. B.D.R. and A.P.M. are thanked for their

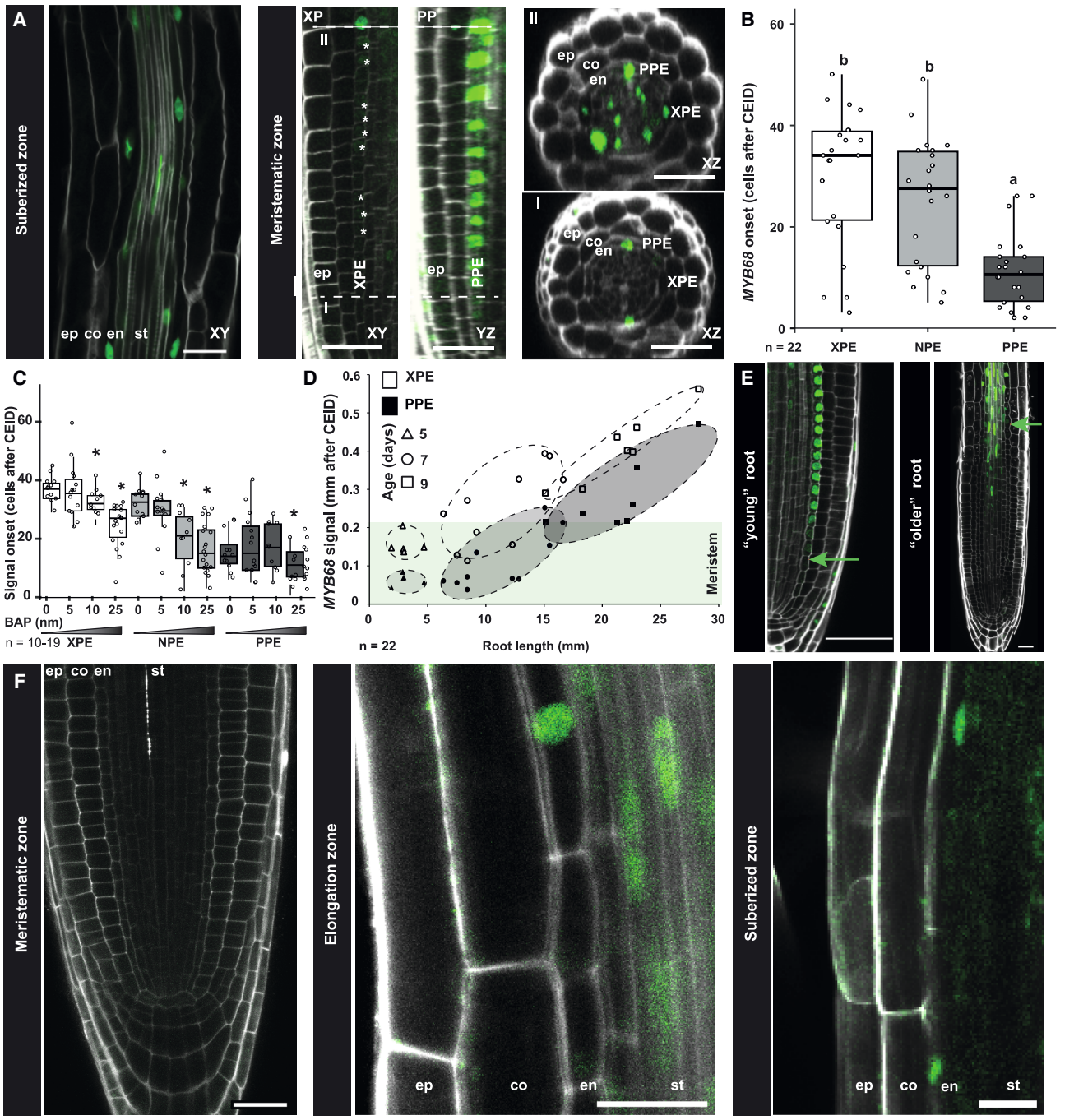

Figure 6. Analysis of MYB68 localization and expression

(A) Activity of *MYB68* in roots of 6-day-old seedlings expressing a transcriptional reporter for *MYB68* activity (*pMYB68*:NLS3xVenus). Cell walls were stained using calcofluor white.[25] Scale bar represents 50 μm. The two dashed lines mark the position of cross-sections I and II.

(B) Analysis of expression onset of *MYB68* in the meristematic zone of plants from (A). Individual letters show significance according to a Kruskal-Wallis test with post hoc Nemenyi test.

(C) Endodermal signal onset of *MYB68* expression in roots of plants grown in the presence of increasing amounts of the artificial cytokinin 6-benzyl-aminopurine (BAP). Asterisks indicate significant differences compared to the untreated sample according to an unpaired Wilcoxon text (*$p < 0.05$).

(D) *MYB68* expression onset in the endodermis.

(E) Images depicting *MYB68* expression start in young (0- to 6-day-old) and older (7- to 9-day-old) roots. Green arrows mark the onset of *MYB68* activity. Scale bar represents 50 μm.

(legend continued on next page)

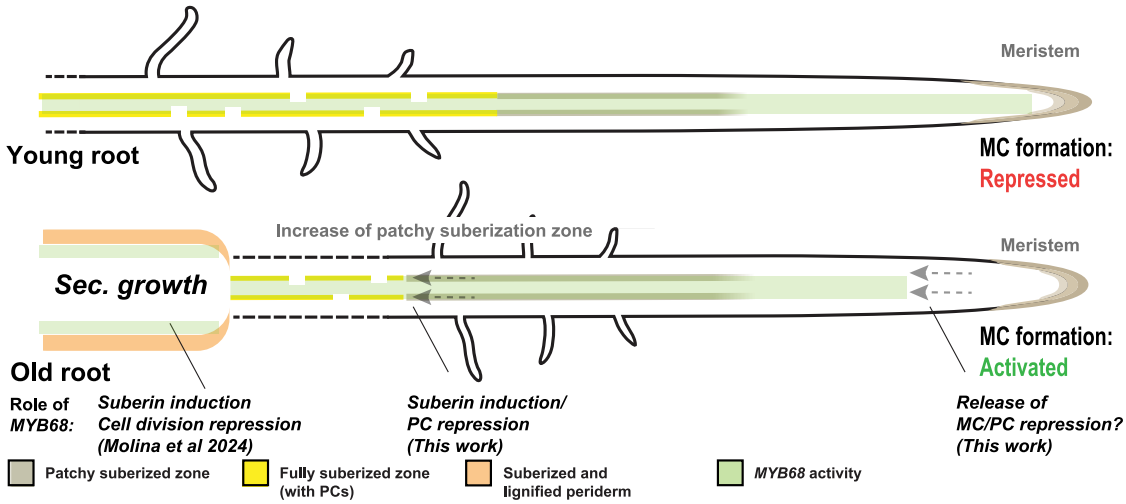

Figure 7. A model of the role of MYB68 in roots at different developmental stages

In young roots (up to 7 days old), *MYB68* shows activity in both meristematic and suberizing regions. In the meristem, our work proposes that it represses periclinal cell divisions in the endodermis, which represses the formation of middle cortex (MC) cells as well as differential steps leading to the formation of endodermal passage cells (PCs). In the suberized zone, MYB68 is likely involved in indirect regulation of the suberization machinery. As the root ages past 7 days (old root), our data support that *MYB68* expression is delayed outside the meristematic region. As a consequence, the absence of the repressing effect of MYB68 on periclinal division in the meristematic region enables MC formation in the xylem pole. This correlates with an observed delay in suberization, which suggests a connection between MC cell and PC formation via MYB68. Moreover, at this stage, the root undergoes secondary growth (sec. growth) and forms the protective periderm via radial divisions. Here, MYB68 serves to control suberization and cell division rate.[19]

reminder of 2024 Post-its. T.G.A. would also like to thank his cat Odin for getting him up early in the morning to work on this manuscript. Research in the lab of T.G.A. is supported by the Sofja Kovalevskaja program from the Alexander von Humboldt Foundation and an independent group leader grant from the Max Planck Society. Research in the lab of L.R. is supported by the Deutsche Forschungsgemeinschaft (DFG) (grant RA2590/4-1 and SFB1101 project B10).

AUTHOR CONTRIBUTIONS

Conceptualization, T.G.A., L.K., and L.R.; methodology, L.K., R.T.N., D.M., L. R., P.F.-J., J.M.M., and T.G.A.; investigation, L.K., R.T.N., and T.G.A.; visualization, L.K., P.F.-J., J.M.M., and T.G.A.; funding acquisition, T.G.A. and L.R.; main writing, T.G.A. and L.K.. All authors read and commented on the final version of the manuscript.

DECLARATION OF INTERESTS

All authors declare that they have no competing interests.

STAR★METHODS

Detailed methods are provided in the online version of this paper and include the following:

SUPPLEMENTAL INFORMATION

Supplemental information can be found online at https://doi.org/10.1016/j.celrep.2025.115794.

Received: May 10, 2024
Revised: March 15, 2025
Accepted: May 15, 2025

REFERENCES

1. Dolan, L., Janmaat, K., Willemsen, V., Linstead, P., Poethig, S., Roberts, K., and Scheres, B. (1993). Cellular organisation of the Arabidopsis thaliana root. Development *119*, 71–84. https://doi.org/10.1242/dev.119.1.71.
2. Geldner, N. (2013). The Endodermis. Annu. Rev. Plant Biol. *64*, 531–558. https://doi.org/10.1146/annurev-arplant-050312-120050.
3. Baum, S.F., Dubrovsky, J.G., and Rost, T.L. (2002). Apical organization and maturation of the cortex and vascular cylinder inArabidopsis thaliana (Brassicaceae) roots. Am. J. Bot. *89*, 908–920. https://doi.org/10.3732/ajb.89.6.908.
4. Paquette, A.J., and Benfey, P.N. (2005). Maturation of the ground tissue of the root is regulated by gibberellin and SCARECROW and requires

(F) Localization of MYB68 (p*MYB68*:GFP-MYB68 in *myb68-2*). Green signal depicts GFP-MYB68, and gray highlights cell walls stained with propidium iodide (PI). For boxplots, the center line indicates the median, dots represent data points, the box limits represent the upper and lower quartiles, and the whiskers represent the maximum and minimum values. Scale bars represent 25 μm. XPE, xylem pole-associated endodermis; PPE, phloem pole-associated endodermis; NPE, non-pole-associated endodermis; ep, epidermis; co, cortex; CEID, cortex endodermis initial daughter cell; en, endodermis; st, stele; XP, xylem pole; PP, phloem pole.

SHORT-ROOT. Plant Physiol. *138*, 636–640. https://doi.org/10.1104/pp.104.058362.

5. Scheres, B., Wolkenfelt, H., Willemsen, V., Terlouw, M., Lawson, E., Dean, C., and Weisbeek, P. (1994). Embryonic origin of the Arabidopsis primary root and root meristem initials. Development *120*, 2475–2487. https://doi.org/10.1242/dev.120.9.2475.
6. Wunderling, A., Ripper, D., Barra-Jimenez, A., Mahn, S., Sajak, K., Targem, M.B., and Ragni, L. (2018). A molecular framework to study periderm formation in Arabidopsis. New Phytol. *219*, 216–229. https://doi.org/10.1111/nph.15128.
7. Caspary, M.R. (1865). Remarks on the protective sheath and on the formation of the stem of the root. Ann. Mag. Nat. Hist. *16*, 382–383. https://doi.org/10.1080/00222936508679451.
8. Priestley, J.H., and North, E.E. (1922). Physiological studies in plant anatomy III. The structure of the endodermis in relation to its function. New Phytol. *21*, 113–139.
9. Franke, R., Briesen, I., Wojciechowski, T., Faust, A., Yephremov, A., Nawrath, C., and Schreiber, L. (2005). Apoplastic polyesters in Arabidopsis surface tissues – A typical suberin and a particular cutin. Phytochemistry *66*, 2643–2658. https://doi.org/10.1016/j.phytochem.2005.09.027.
10. Sitte, P. (1959). Mischkörperdoppelbrechung der Kork-Zellwände. Naturwissenschaften *46*, 260–261. https://doi.org/10.1007/BF00632301.
11. Andersen, T.G., Barberon, M., and Geldner, N. (2015). Suberization - the second life of an endodermal cell. Curr. Opin. Plant Biol. *28*, 9–15. https://doi.org/10.1016/j.pbi.2015.08.004.
12. Alassimone, J., Naseer, S., and Geldner, N. (2010). A developmental framework for endodermal differentiation and polarity. Proc. Natl. Acad. Sci. USA *107*, 5214–5219. https://doi.org/10.1073/pnas.0910772107.
13. Andersen, T.G., Naseer, S., Ursache, R., Wybouw, B., Smet, W., De Rybel, B., Vermeer, J.E.M., and Geldner, N. (2018). Diffusible repression of cytokinin signalling produces endodermal symmetry and passage cells. Nature *555*, 529–533. https://doi.org/10.1038/nature25976.
14. Holbein, J., Shen, D., and Andersen, T.G. (2021). The endodermal passage cell – just another brick in the wall? New Phytol. *230*, 1321–1328. https://doi.org/10.1111/nph.17182.
15. Peterson, C.A., and Enstone, D.E. (1996). Functions of passage cells in the endodermis and exodermis of roots. Physiol. Plantarum *97*, 592–598. https://doi.org/10.1111/j.1399-3054.1996.tb00520.x.
16. Mähönen, A.P., Bishopp, A., Higuchi, M., Nieminen, K.M., Kinoshita, K., Törmäkangas, K., Ikeda, Y., Oka, A., Kakimoto, T., and Helariutta, Y. (2006). Cytokinin signaling and its inhibitor AHP6 regulate cell fate during vascular development. Science *311*, 94–98. https://doi.org/10.1126/science.1118875.
17. Liberman, L.M., Sparks, E.E., Moreno-Risueno, M.A., Petricka, J.J., and Benfey, P.N. (2015). MYB36 regulates the transition from proliferation to differentiation in the *Arabidopsis* root. Proc. Natl. Acad. Sci. USA *112*, 12099–12104. https://doi.org/10.1073/pnas.1515576112.
18. Kamiya, T., Borghi, M., Wang, P., Danku, J.M.C., Kalmbach, L., Hosmani, P.S., Naseer, S., Fujiwara, T., Geldner, N., and Salt, D.E. (2015). The MYB36 transcription factor orchestrates Casparian strip formation. Proc. Natl. Acad. Sci. USA *112*, 10533–10538. https://doi.org/10.1073/pnas.1507691112.
19. Molina, D., Horvath, S., Zhang, X., Xiao, W., Ragab, N., Ripper, D., Kilian, J., Andersen, T.G., and Ragni, L. (2024). MYB68 orchestrates cork differentiation by regulating stem cell proliferation and suberin deposition. Preprint at bioRxiv. https://doi.org/10.1101/2024.03.06.583666.
20. Feng, C., Andreasson, E., Maslak, A., Mock, H.P., Mattsson, O., and Mundy, J. (2004). Arabidopsis MYB68 in development and responses to environmental cues. Plant Sci. *167*, 1099–1107. https://doi.org/10.1016/j.plantsci.2004.06.014.
21. Naseer, S., Lee, Y., Lapierre, C., Franke, R., Nawrath, C., and Geldner, N. (2012). Casparian strip diffusion barrier in *Arabidopsis* is made of a lignin polymer without suberin. Proc. Natl. Acad. Sci. USA *109*, 10101–10106. https://doi.org/10.1073/pnas.1205726109.
22. Doblas, V.G., Smakowska-Luzan, E., Fujita, S., Alassimone, J., Barberon, M., Madalinski, M., Belkhadir, Y., and Geldner, N. (2017). Root diffusion barrier control by a vasculature-derived peptide binding to the SGN3 receptor. Science *355*, 280–284. https://doi.org/10.1126/science.aaj1562.
23. Barberon, M., Vermeer, J.E.M., De Bellis, D., Wang, P., Naseer, S., Andersen, T.G., Humbel, B.M., Nawrath, C., Takano, J., Salt, D.E., and Geldner, N. (2016). Adaptation of Root Function by Nutrient-Induced Plasticity of Endodermal Differentiation. Cell *164*, 447–459. https://doi.org/10.1016/j.cell.2015.12.021.
24. Serra, O., Mähönen, A.P., Hetherington, A.J., and Ragni, L. (2022). The Making of Plant Armor: The Periderm. Annu. Rev. Plant Biol. *73*, 405–432. https://doi.org/10.1146/annurev-arplant-102720-031405.
25. Ursache, R., Andersen, T.G., Marhavý, P., and Geldner, N. (2018). A protocol for combining fluorescent proteins with histological stains for diverse cell wall components. Plant J. *93*, 399–412. https://doi.org/10.1111/tpj.13784.
26. Hamburger, D., Rezzonico, E., MacDonald-Comber Petétot, J., Somerville, C., and Poirier, Y. (2002). Identification and characterization of the Arabidopsis PHO1 gene involved in phosphate loading to the xylem. Plant Cell *14*, 889–902. https://doi.org/10.1105/tpc.000745.
27. Zhou, Y., Zhou, B., Pache, L., Chang, M., Khodabakhshi, A.H., Tanaseichuk, O., Benner, C., and Chanda, S.K. (2019). Metascape provides a biologist-oriented resource for the analysis of systems-level datasets. Nat. Commun. *10*, 1523. https://doi.org/10.1038/s41467-019-09234-6.
28. Osakabe, Y., Arinaga, N., Umezawa, T., Katsura, S., Nagamachi, K., Tanaka, H., Ohiraki, H., Yamada, K., Seo, S.-U., Abo, M., et al. (2013). Osmotic Stress Responses and Plant Growth Controlled by Potassium Transporters in Arabidopsis. Plant Cell *25*, 609–624. https://doi.org/10.1105/tpc.112.105700.
29. Gierth, M., Mäser, P., and Schroeder, J.I. (2005). The potassium transporter AtHAK5 functions in K(+) deprivation-induced high-affinity K(+) uptake and AKT1 K(+) channel contribution to K(+) uptake kinetics in Arabidopsis roots. Plant Physiol. *137*, 1105–1114. https://doi.org/10.1104/pp.104.057216.
30. Mäser, P., Eckelman, B., Vaidyanathan, R., Horie, T., Fairbairn, D.J., Kubo, M., Yamagami, M., Yamaguchi, K., Nishimura, M., Uozumi, N., et al. (2002). Altered shoot/root Na+ distribution and bifurcating salt sensitivity in Arabidopsis by genetic disruption of the Na+ transporter AtHKT1. FEBS Lett. *531*, 157–161. https://doi.org/10.1016/s0014-5793(02)03488-9.
31. Oliva, M., Stuart, T., Tang, D., Pflueger, J., Poppe, D., Jabbari, J.S., Gigante, S., Dragwidge, J.M., Whelan, J., Lewsey, M.G., and Lister, R. (2022). An environmentally-responsive transcriptional state modulates cell identities during root development. Preprint at bioRxiv. https://doi.org/10.1101/2022.03.04.483008.
32. Yoshida, H., Hirano, K., Sato, T., Mitsuda, N., Nomoto, M., Maeo, K., Koketsu, E., Mitani, R., Kawamura, M., Ishiguro, S., et al. (2014). DELLA protein functions as a transcriptional activator through the DNA binding of the indeterminate domain family proteins. Proc. Natl. Acad. Sci. USA *111*, 7861–7866. https://doi.org/10.1073/pnas.1321669111.
33. Zhang, Z.-L., Ogawa, M., Fleet, C.M., Zentella, R., Hu, J., Heo, J.-O., Lim, J., Kamiya, Y., Yamaguchi, S., and Sun, T.-p. (2011). SCARECROW-LIKE 3 promotes gibberellin signaling by antagonizing master growth repressor DELLA in Arabidopsis. Proc. Natl. Acad. Sci. USA *108*, 2160–2165. https://doi.org/10.1073/pnas.1012232108.
34. Millard, P.S., Weber, K., Kragelund, B.B., and Burow, M. (2019). Specificity of MYB interactions relies on motifs in ordered and disordered contexts. Nucleic Acids Res. *47*, 9592–9608. https://doi.org/10.1093/nar/gkz691.
35. De Rybel, B., Mähönen, A.P., Helariutta, Y., and Weijers, D. (2016). Plant vascular development: from early specification to differentiation. Nat. Rev. Mol. Cell Biol. *17*, 30–40. https://doi.org/10.1038/nrm.2015.6.

36. Lee, H.G., and Seo, P.J. (2016). The Arabidopsis MIEL1 E3 ligase negatively regulates ABA signalling by promoting protein turnover of MYB96. Nat. Commun. *7*, 12525. https://doi.org/10.1038/ncomms12525.

37. Yang, B., Sun, Y., Minne, M., Ge, Y., Yue, Q., Goossens, V., Mor, E., Callebaut, B., Bevernaege, K., Winne, J.M., et al. (2024). SPL13 controls a root apical meristem phase change by triggering oriented cell divisions. Science *386*, eado4298. https://doi.org/10.1126/science.ado4298.

38. Lin, Y.F., Liang, H.M., Yang, S.Y., Boch, A., Clemens, S., Chen, C.C., Wu, J.F., Huang, J.L., and Yeh, K.C. (2009). Arabidopsis IRT3 is a zinc-regulated and plasma membrane localized zinc/iron transporter. New Phytol. *182*, 392–404. https://doi.org/10.1111/j.1469-8137.2009.02766.x.

39. Gaymard, F., Pilot, G., Lacombe, B., Bouchez, D., Bruneau, D., Boucherez, J., Michaux-Ferrière, N., Thibaud, J.B., and Sentenac, H. (1998). Identification and disruption of a plant shaker-like outward channel involved in K+ release into the xylem sap. Cell *94*, 647–655. https://doi.org/10.1016/s0092-8674(00)81606-2.

40. Cui, H. (2015). Cortex proliferation in the root is a protective mechanism against abiotic stress. Plant Signal. Behav. *10*, e1011949. https://doi.org/10.1080/15592324.2015.1011949.

41. Chen, S., Zhou, Y., Chen, Y., and Gu, J. (2018). fastp: an ultra-fast all-in-one FASTQ preprocessor. Bioinformatics *34*, i884–i890. https://doi.org/10.1093/bioinformatics/bty560.

42. Kim, D., Paggi, J.M., Park, C., Bennett, C., and Salzberg, S.L. (2019). Graph-based genome alignment and genotyping with HISAT2 and HISAT-genotype. Nat. Biotechnol. *37*, 907–915. https://doi.org/10.1038/s41587-019-0201-4.

43. Liao, Y., Smyth, G.K., and Shi, W. (2014). featureCounts: an efficient general purpose program for assigning sequence reads to genomic features. Bioinformatics *30*, 923–930. https://doi.org/10.1093/bioinformatics/btt656.

44. Robinson, M.D., McCarthy, D.J., and Smyth, G.K. (2010). edgeR: a Bioconductor package for differential expression analysis of digital gene expression data. Bioinformatics *26*, 139–140. https://doi.org/10.1093/bioinformatics/btp616.

45. Andersen, T.G., Molina, D., Kilian, J., Franke, R.B., Ragni, L., and Geldner, N. (2021). Tissue-autonomous phenylpropanoid production is essential for establishment of root barriers. Curr. Biol. *31*, 965–977.e5.

46. Logemann, E., Birkenbihl, R.P., Ülker, B., and Somssich, I.E. (2006). An improved method for preparing Agrobacterium cells that simplifies the Arabidopsis transformation protocol. Plant Methods *2*, 16. https://doi.org/10.1186/1746-4811-2-16.

47. Shimada, T.L., Shimada, T., and Hara-Nishimura, I. (2010). A rapid and non-destructive screenable marker, FAST, for identifying transformed seeds of Arabidopsis thaliana. Plant J. *61*, 519–528. https://doi.org/10.1111/j.1365-313X.2009.04060.x.

48. LUX, A., MORITA, S., ABE, J., and ITO, K. (2005). An Improved Method for Clearing and Staining Free-hand Sections and Whole-mount Samples. Ann. Bot. *96*, 989–996. https://doi.org/10.1093/aob/mci266.

49. Sexauer, M., Shen, D., Schön, M., Andersen, T.G., and Markmann, K. (2021). Visualizing polymeric components that define distinct root barriers across plant lineages. Development *148*, dev199820. https://doi.org/10.1242/dev.199820.

50. Cheng, C.Y., Krishnakumar, V., Chan, A.P., Thibaud-Nissen, F., Schobel, S., and Town, C.D. (2017). Araport11: a complete reannotation of the Arabidopsis thaliana reference genome. Plant J. *89*, 789–804. https://doi.org/10.1111/tpj.13415.

51. Oliva, M., Stuart, T., Tang, D., Pflueger, J., Poppe, D., Jabbari, J.S., Gigante, S., Dragwidge, J.M., Whelan, J., Lewsey, M.G., and Lister, R. (2022). An environmentally responsive transcriptional state modulates cell identities during root development. Preprint at bioRxiv. https://doi.org/10.1101/2022.03.04.483008.

STAR★METHODS

KEY RESOURCES TABLE

REAGENT or RESOURCE	SOURCE	IDENTIFIER
Experimental models: Organisms/strains		
myb68-2	This paper	N/A
myb68-3	This paper	N/A
myb36-2	Liberman et al.[17]	N/A
myb37-1	Molina et al.[19]	N/A
myb38-2	Molina et al.[19]	N/A
myb84-1	Molina et al.[19]	N/A
myb87-3a	Molina et al.[19]	N/A
p*GPAT5*:mCitrine-SYP122 p*PHO1;H3*:NLS 3xmVenus (2 independent lines)	This paper	N/A
myb68-2 pPHO1;H3:NLS 3xmVenus (3 independent lines)	This paper	N/A
Col-0 *pKUP8*:NLS3xVenus (3 independent lines)	This paper	N/A
Col-0 *pHKT1*:NLS3xmScarlet (2 independent lines)	This paper	N/A
myb68-2 pKUP8:NLS3xVenus (3 independent lines)	This paper	N/A
myb68-2 pHKT1:NLS3xmScarlet (3 independent lines)	This paper	N/A
Col-0 *pMYB68*:NLS3xVenus (2 independent lines)	This paper	N/A
myb68-2 pMYB68:GFP-MYB68	This paper	N/A
myb68-2 pMYB68: FLAG-MYB68	This paper	N/A
Accession numbers	www.arabidopsis.org	
HAK5	www.arabidopsis.org	At4g13420
HKT1	www.arabidopsis.org	At4g10310
MYB36	www.arabidopsis.org	At5g57620
MYB37	www.arabidopsis.org	At5g57620
MYB38	www.arabidopsis.org	At2g36890
MYB68	www.arabidopsis.org	At5g65790
MYB84	www.arabidopsis.org	At4g37780
MYB87	www.arabidopsis.org	At3g49690
KUP8	www.arabidopsis.org	At5g14880
PHO1;H3	www.arabidopsis.org	At1g14040
RGL3	www.arabidopsis.org	At5g17490
SCL3	www.arabidopsis.org	At1g50420
Critical commercial assays		
BP clonase II	Invitrogen	N/A
LR clonase II	Invitrogen	N/A
Infusion cloning	Takara	N/A
ReliaPrep RNA extraction kit	Promega	Z6012
Illumina NovaSeq platform	Novogene	N/A
HAK5 probe	Molecular Instruments	LOT #RTI354
B3h1 (hairpin)	Molecular Instruments	LOT #S073325
B3h2 (hairpin)	Molecular Instruments	LOT #S075725

(*Continued on next page*)

Continued		
REAGENT or RESOURCE	SOURCE	IDENTIFIER
Bacillus subtilis dapB gene probe	Molecular Instruments	LOT #RTB 421
B1h1 (hairpin)	Molecular Instruments	LOT #S046325
B1h2 (hairpin)	Molecular Instruments	LOT #S050925
HKT1 probe	Molecular Instruments	LOT #RTG433
Deposited data		
RNA Seq	This paper	BioProjectID: PRJNA1110212
Oligonucleotides		
Primer for cloning constructs in recombinant DNA section Table S6	This paper	N/A
Recombinant DNA		
pUC19 entry vector	Invitrogen	N/A
pDONR221 entry vector	Invitrogen	N/A
pED97	Andersen et al.[13]	N/A
pPHO1;H3:NLS 3xmVenus	Andersen et al.[13]	N/A
pKUP8:NLS3xVenus	This paper	N/A
pHKT1:NLS3xmScarlet	This paper	N/A
pMYB68:NLS3xVenus	This paper	N/A
pMYB68:GFP-MYB68	This paper	N/A
pMYB68: FLAG-MYB68	This paper	N/A
Chemicals, peptides, and recombinant proteins		
N6 Benzyladenine	Sigma Aldrich	CAS #1214-39-7
Abscisic acid	Sigma Aldrich	CAS #21293-29-8
Murashige and Skoog Medium	Duchefa	N/A
Bacto Agar	Duchefa	CAS #9002-18-0
Flourol Yellow 088	Interchim	CAS #586-39-0
Aniline blue	Sigma Aldrich	CAS #66687-07-8
Paraformaldehyde	Sigma Aldrich	CAS #30525-89-4
Xylitol	Roth	CAS #87-99-0
Sodium deoxycholate	Thermo scientific	CAS #302-95-4
Urea	Roth	CAS #57-13-6
Propidium iodide	Sigma Aldrich	CAS #25535-16-4
Calcofluor white (Fluorescent Brightener 28)	Sigma Aldrich	CAS #4404-43-7
Formaldehyde	Sigma Aldrich	CAS #50-00-0
Bacterial and virus strains		
Escherichia coli	N/A	TOP10
Agrobacterium tumefaciens	N/A	GV3101
Software and algorithms		
Fastp	Chen et al.[41]	N/A
HISAT2	Kim et al.[42]	N/A
FeatureCounts	Liao et al.[43]	N/A
R software	https://www.r-project.org/	N/A
edgeR package	Robinson et al.[44]	N/A
Metascape	Zhou et al.[27]	N/A

EXPERIMENTAL MODEL AND STUDY PARTICIPANT DETAILS

In this study Arabidopsis ecotype Columbia-0 was used. Plants were grown, if not otherwise stated for 5–7 days at long day (16h) and 21°C in 140 µmol/m^2/s on ½ MS (Duchefa) 0.8% agar (Bacto Agar) 5.8 pH. For cytokinin treatment, seeds were germinated on ½ MS

plates, containing 5,10 or 25 nM N^6 Benzyladenine (CAS #1214-39-7). For abscisic acid (ABA) treatment 5–day–old seedlings were transferred to ½ MS plates containing 1 μM ABA (CAS # 21293-29-8) and grown for 2 days.

METHOD DETAILS

Cloning

To generate the transcription reporter lines, the corresponding promoters (amplified using primer listed in Table S6) were inserted into a modified pUC19 entry vector[45] via Infusion cloning (Takara) according to the manufacturer description. The coding sequences of the fluorescent protein and the nuclear localization signal or MYB68 were inserted into a pDONR221 entry vector using BP clonase II (Invitrogen) and recombined using LR clonase II (Invitrogen) into the destination vector pED97 containing a FastRed selection.[13] All constructs were transformed into plants using a modified floral dip method[46] and selected for FastRed[47] before propagating further. All mutants in MYB genes were described previously.[19]

Staining procedures

For overall suberin pattern analysis, seedlings were stained in 0.01% Flourol Yellow 088 solution (w/v) (interchim) in lactic acid for 30 min at 70°C, washed and counterstained in a 0.5% Aniline blue solution (CAS # 66687-07-8) (w/v) in water for 30 min at room temperature.[21,48] For radial suberin pattern analysis seedlings were fixed in 4% paraformaldehyde (PFA) (CAS # 30525-89-4), cleared with Clearsee (10% xylitol (w/v) (Roth CAS 87-99-0), 15% sodium deoxycholate (w/v) (Thermo scientific CAS # 302-95-4) and 25% urea (w/v) (Roth CAS # 57-13-6) and stained with 0.01% Fluorol Yellow dissolved in Ethanol as described previously.[49] For Casparian strip integrity analysis, seedlings were incubated in a 10 μg/mL propidium iodide (Sigma Aldrich CAS #25535-16-4) dissolved in water and washed with water before imaging.[21] For analysis of transcriptional reporter lines, cell length and middle cortex quantification, seedlings were fixed, cleared and stained with 0.1% calcofluor white (Fluorescent Brightener 28 CAS #4404-43-7) dissolved in clearesee.[25]

Transcriptional analysis

For transcriptomic analysis of wild-type and *myb68-2* roots, plants were grown in the presence of mock (DMSO) or 25 nM BAP for 6 days under long day conditions. Total RNA from pooled roots was extracted using a Trizol (Invitrogen) adapted ReliaPrep RNA extraction kit (Promega, Z6012) and subjected to quality control, library preparation, and sequencing on the Illumina NovaSeq platform (Novogene). Approximately 25,000,000 reads (150-bp paired-end), on average, were obtained per sample. Raw reads were processed and cleaned up using fastp[41] with default settings mapped to *A. thaliana* Col-0 genome with the latest annotation[50] using HISAT2[42] with default parameters for paired-end reads. Reads per gene without consideration of splicing variants were counted by featureCounts[43] with default parameters. Subsequent statistical analyses were performed using R software (https://www.r-project.org/) unless described otherwise. Differential expression analysis was performed using the *edgeR* package.[44] Library size was normalized by the weighted trimmed mean of M-values (TMM) method, and normalized read counts were fitted to a generalized linear model (GLM) with a negative binomial distribution to identify significantly DEGs. GO enrichment analysis was performed by Metascape.[27]

Fluorescent *in situ* hybridization

In situ hybridization chain reaction was performed according to.[51] In short, 6-day old roots were fixed with formaldehyde (CAS # 50-00-0) and dehydrated with a series of increasing concentrations of ethanol and incubation at 100% methanol at −20°C overnight. After rehydration with a decreasing series of methanol concentrations, cell wall was digested in a solution containing cellulase, pectolyase, macerozyme and pectinase at room temperature for 15 min. After proteinase K incubation and additional fixation steps, probe hybridization (*HAK5* probe LOT # RTI354, Molecular Instruments) was performed overnight at 37°C. After washing, 10 μL of 3 μM of B3h1 (LOT#S073325, Molecular Instruments) and H2 (LOT#S075725, Molecular Instruments) hairpin solution was added in amplification buffer, allowing amplification at room temperature for 16 h. As negative controls either a probe specific for the Bacillus subtilis dapB gene (LOT # RTB 421, Molecular Instruments) with the corresponding amplifier B1h1 (LOT #S046325, Molecular Instruments) and B1h2 (LOT #S050925, Molecular Instruments) or just the amplifier used for *HAK5* B3h1 (LOT#S073325, Molecular Instruments) and B3h2 (LOT#S075725, Molecular Instruments) without a probe were used. Excess hairpin was washed away, seedlings were cleared with Clearsee (10% xylitol (w/v) (Roth CAS 87-99-0), 15% sodium deoxycholate (w/v) (Thermo scientific CAS 302-95-4) and 25% urea (w/v) (Roth CAS # 57-13-6) and stained with calcofluor white (Fluorescent Brightener 28 CAS #4404-43-7).

Microscopy/imaging

Endodermal suberin patterning was imaged with an AxioZoom V16 using a standard GFP filtercube. The parts of the root were defined as follows: Unsuberized zone: from root tip to first suberized cell; patchy zone: from first suberized cell to the first point where all cells across the circumference of the endodermis are suberized; fully suberized zone: from first ring of suberized cells to the root-hypocotyl junction. Suberin radial pattern, middle cortex, transcriptional marker lines and FISH samples were imaged with a confocal laser scanning microscope (Zeiss LSM 980) with the following settings: flourol yellow (ex: 488 nm, em: 500–550 nm), propidium iodide (ex: 561 nm, em: 600–650 nm), calcofluor white (ex: 405 nm, em: 407–466 nm),Venus transcriptional marker line (ex: 514 nm,

em: 500–560 nm), Scarlett signal (ex: 561 nm, em: 570–640 nm), FISH samples (ex: 639 nm, em: 650-680nm). Confocal images were taken with the 40x (NA 1.2) oil immersion objective and Zen Connect was used to determine the exact position of the image in the root.

Radial suberization pattern analysis

We constructed one-dimensional arrays for each cell file, and assigned the values 1 and 0 to each suberized and unsuberized cell, respectively. We first normalized the length of all arrays to an arbitrary size (we choose $N = 2000$ units), a procedure that allows the direct comparison between cell files and roots with different cell number. After this rescaling, all arrays have the same length, but the size of the corresponding cells has changed (Figure 2A). To analyze the progression of suberization along different cell files, we computed the normalized cumulative sum CS_i of the rescaled arrays, defined as $CS_i = \frac{1}{N}\sum_{j=0}^{i} A_j$, where CS_i is the i-th element of the cumulative sum, N is the length of the array, A_j are the entries of the suberin arrays (e.g., $A_j = [0,0,1,0,1,\ldots,1,1,1]$), and index j runs from 0, the start of the array, to the i-th element of the array. The cumulative sum progressively adds the contributions of every suberized cell, reaching a final value that will depend on the number of 1s and 0s in the array. For instance, for a completely suberized root, the normalized cumulative sum will take the form $\left[\frac{1}{N}, \frac{2}{N}, \frac{3}{N}, \ldots, 1\right]$, reaching a maximum value of 1. The cumulative sum is a strictly non-decreasing function, and its final value represents the proportion of suberized cells of an array.

QUANTIFICATION AND STATISTICAL ANALYSIS

Statistical analysis was performed in R. Datasets were analyzed for normal distribution using the Shapiro-Wilk test. In case data was normally distributed One-way Anova with post hoc Tukey's HSD test was performed for multiple comparisons and Students T test or Welch two sample test was performed for comparison of two groups. In case data was not normally distributed for multiple comparison Kruskal Wallis test with post hoc Nemenyi test was used and for comparison of two groups unpaired Wilcoxon test was employed. For time-course experiments linear regression analysis was conducted. All analysis were performed at least twice in independent experiments.